Catalytic Ammonia Oxidation to Dinitrogen by a Nickel Complex

David N. Stephens[a], Robert K. Szilagyi[b], Paige N. Roehling[a], Navamoney Arulsamy[c], and Michael T. Mock*[a]

[a] D. N. Stephens, P. N. Roehling, Prof. M. T. Mock
Department of Chemistry and Biochemistry
Montana State University
Bozeman, Montana 59717, USA
E-mail: michael.mock@montana.edu

[b] Prof. Robert K. Szilagyi
Department of Chemistry
University of British Columbia, Okanagan
Kelowna, British Columbia, Canada
E-mail: robert.szilagyi@ubc.ca

[c] Dr. Navamoney Arulsamy
Department of Chemistry
University of Wyoming
Laramie, Wyoming 82071, USA
E-mail: Arulsamy@uwyo.edu

Supporting information for this article is given via a link at the end of the document

Abstract: We report a nickel complex for catalytic oxidation of ammonia to dinitrogen under ambient conditions. Using the aryloxyl radical 2,4,6-tri-*tert*-butylphenoxyl (^{t}Bu$_3$ArO$^\bullet$) as H atom acceptor to cleave the N-H bond of a coordinated NH_3 ligand up to 56 equiv of N_2 per Ni center can be generated. Employing the *N*-oxyl radical 2,2,6,6-(tetramethylpiperidin-1-yl)oxyl (TEMPO$^\bullet$) as the H-atom acceptor, ~15 equiv of N_2 per Ni center are formed. A bridging Ni-hydrazine product identified by isotopic nitrogen (^{15}N) studies and supported by computational models indicates the N–N bond forming step occurs by bimetallic homocoupling of two paramagnetic Ni-NH_2 fragments. Ni-mediated hydrazine disproportionation to N_2 and NH_3 completes the catalytic cycle.

Ammonia (NH_3) has garnered global attention as a large-scale sustainable energy carrier due to its high energy density, ease of distribution, storage, and potential use as a transportation fuel.[1] A drawback is the large scale NH_3 synthesis by the Haber-Bosch process imparting a significant carbon footprint.[2] However, efficient, and potentially carbon-free methods for NH_3 synthesis using renewable energy are on the horizon.[3] Such advancements have the potential to change the landscape for worldwide energy production and utilization from carbon-based fuels toward a nitrogen-centric energy economy.[4]

The study of molecular catalysts for NH_3 oxidation provides a mechanistic understanding of the reaction steps required to convert the energy stored in N–H bonds into electrical or chemical energy through H_2 (and N_2) when NH_3 is utilized as a fuel.[5] Critical to catalyst development is how to efficiently mediate the challenging cleavage of up to six N-H bonds and the formation of an N–N bond en route to N_2 formation.[6] In 2019 Hamann, Smith, and coworkers described electrocatalytic NH_3 oxidation using a Ru polypyridyl complex.[7] Since this seminal report, electrocatalytic NH_3 oxidation has been demonstrated by Ru,[8] Fe,[9] and Mn[10] complexes. A 2021 report of an Fe complex with a polypyridyl ligand formed up to 149 equiv of N_2 per Fe center.[9b]

Ru complexes that *chemically* catalyze the oxidation of NH_3 to N_2 were among the early systems reported in 2019. Sakata Nishibayashi, and coworkers utilized a chemical oxidant and a base to cleave N–H bonds of NH_3 using a Ru catalyst supported

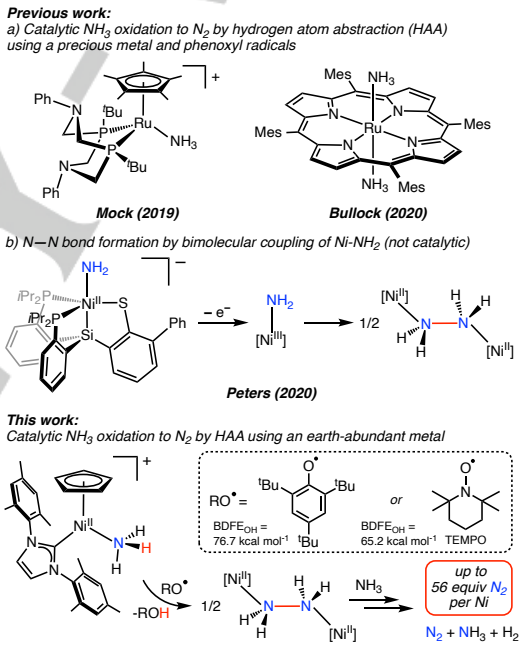

Figure 1. Top: Molecular catalysts utilizing Ru and phenoxyl radicals for catalytic NH_3 oxidation to N_2. Middle: a mechanistic study describing bimetallic coupling of Ni–NH_2 to form an N–N bond. Bottom: Catalytic NH_3 oxidation to N_2 using Ni and organic radicals as H atom acceptors described in this work. (Mes = mesityl; O-H bond dissociation free energies ($BDFE_{OH}$) shown above reported in benzene.[11])

by 2,2′-bipyridyl-6,6′-dicarboxylate ligands.[8c] In an alternative approach, we employed the 2,4,6-tri-*tert*-butylphenoxyl radical (^{t}Bu$_3$ArO$^\bullet$) to catalyze NH_3 oxidation to N_2 by homolytic N–H bond cleavage,[12] i.e. hydrogen atom abstraction (HAA) using a [Cp*Ru(diphosphine)(NH_3)]$^+$ complex,[13] Figure 1a. In 2020, Bullock and coworkers used a similar strategy with a Ru porphyrin complex for catalytic NH_3 oxidation.[14] Using organic radicals to cleave N–H bonds of NH_3 has a practical benefit as the radical could be regenerated electrochemically from the ROH product as part of an overall catalytic cycle.[6, 15]

While Ru has been the choice in a majority of chemical NH_3 oxidation catalysts, examples using earth-abundant metals are

rare. Recently, Nishibayashi, Sakata, and coworkers reported chemical and electrocatalytic NH_3 oxidation to N_2 using a Mn salen complex.[10] Brudvig and coworkers reported a copper electrocatalyst for the oxidization of NH_3 to nitrite and nitrate using aqueous conditions.[16] In a related mechanistic study, Peters and coworkers demonstrated the N–N bond forming step by the bimolecular coupling of two Ni–NH_2 fragments to form a dinuclear Ni hydrazine complex (Figure 1b) in an overall synthetic cycle for NH_3 oxidation.[17] Herein, we describe catalytic NH_3 oxidation to N_2 using the Ni complex [CpNi(IMes)(NH_3)][X] X = PF_6 or $BAr^F{}_{24}$ (**1-PF$_6$** or **1-BAr$^F{}_{24}$**) (Cp = C_5H_5; IMes = 1,3-Bis(2,4,6-trimethylphenyl)-1,3-dihydro-2H-imidazol-2-ylidene; $Ar^F{}_{24}$ = 3,5-$(CF_3)_2C_6H_3$). We show that ^{t}Bu$_3$ArO$^\bullet$ *or* TEMPO$^\bullet$ radical can be used as the H atom acceptor to catalytically generate N_2, Figure 1. In the proposed catalytic cycle supported by computational modeling, the N–N bond forming step occurs by the bimolecular coupling of two Ni–NH_2 fragments.

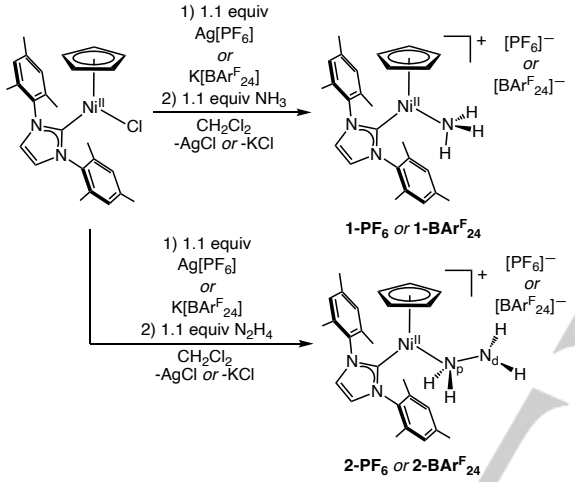

Scheme 1. Synthesis of complexes [CpNi(IMes)(NH_3)][X]; X = PF_6 or $BAr^F{}_{24}$ (**1-PF$_6$** or **1-BAr$^F{}_{24}$**) and [CpNi(IMes)(N_2H_4)][X]; X = PF_6 or $BAr^F{}_{24}$ (**2-PF$_6$** or **2-BAr$^F{}_{24}$**).

Treatment of a red dichloromethane (CH_2Cl_2) solution of CpNiCl(IMes)[18] with 1.1 equiv of $AgPF_6$ or $KBAr^F{}_{24}$ followed by addition of NH_3 affords the yellow cationic Ni complexes **1-PF$_6$** or **1-BAr$^F{}_{24}$**, respectively (Scheme 1). Similarly, the yellow complexes [CpNi(IMes)(N_2H_4)][X] X = PF_6 or $BAr^F{}_4$ (**2-PF$_6$** or **2-BAr$^F{}_{24}$**) are prepared by addition of N_2H_4 to a CH_2Cl_2 solution of CpNiCl(IMes) and 1.1 equiv of $AgPF_6$ or $KBAr^F{}_{24}$.

The ^{1}H resonance corresponding to the coordinated NH_3 ligand in **1-BAr$^F{}_{24}$** exhibits solvent dependent chemical shifts. For example, a broad singlet is observed at δ 0.42 ppm in CD_2Cl_2, and in C_6D_6 the Ni-N*H*$_3$ resonance appears at δ-0.98 ppm. **1-PF$_6$** is insoluble in C_6D_6. A sample prepared using $^{15}NH_3$ gas, [CpNi(IMes)($^{15}NH_3$)][$BAr^F{}_{24}$]; (**1^{15N}-BAr$^F{}_{24}$**) affords a doublet ($J_{15N\text{-}H}$ = 69 Hz) in the ^{1}H NMR spectrum for Ni–^{15}N*H*$_3$ and ^{15}N resonance at δ -457 ppm in C_6D_6 (δ -451 ppm in CD_2Cl_2) corroborated by the ^{1}H-^{15}N HSQC spectrum. The ^{1}H NMR spectrum of **2-BAr$^F{}_{24}$** in CD_2Cl_2 revealed two broad resonances at δ 2.56 ppm and δ 3.11 ppm (^{15}N cross-peaks at δ -308 ppm and δ -395 ppm, respectively, in the ^{1}H-^{15}N HSQC spectrum) for the distal N_d and proximal N_p atoms, i.e. Ni-N_pH_2-N_dH_2, respectively.

The solid-state structures[19] of **1-PF$_6$** and **1-BAr$^F{}_{24}$** from single crystal X-ray diffraction confirmed the presence of the NH_3 ligand coordinated to Ni with comparable Ni–N bond distances of 1.951(3) Å and 1.9476(12) Å, respectively (Figure 2). Likewise, the structure of **2-PF$_6$** shows the coordinated hydrazine moiety with a Ni–N_p bond length of 1.9373(11) Å and a N_p–N_d distance of 1.4636(14) Å. The crystal structures of **1-PF$_6$**, **1-BAr$^F{}_{24}$**, and **2-PF$_6$** reveal discrete interactions (*ca.* <3.0 Å) between the Ni-NH_3 or Ni-N_2H_4 hydrogen atoms and the CF_3 groups of $[BAr^F{}_{24}]^-$ or the $[PF_6]^-$ ion (See Supporting Information, SI).

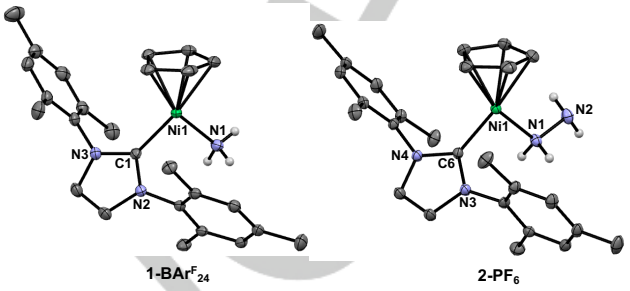

Figure 2. Molecular structures of the cation of **1-BAr$^F{}_{24}$** [CpNi(IMes)(NH_3)]$^+$ and [CpNi(IMes)(N_2H_4)]$^+$ **2-PF$_6$**. Hydrogen atoms (except for N-ligands), $BAr^F{}_{24}$ and PF_6 anions, and solvent molecules omitted for clarity. Thermal ellipsoids shown at 50% probability level. Selected bond lengths [Å] and angles [°]: **1-BAr$^F{}_{24}$** Ni1-N1: 1.9476(12), Ni1-C1: 1.8932(12); C1-Ni1-N3: 98.00(5). **2-PF$_6$** Ni1-N1: 1.9373(11), Ni1-C6: 1.8924(11), N1-N2: 1.4636(14); C6-Ni1-N1: 95.54(5).

In solid-state or in non-coordinating solvents **1-PF$_6$** and **1-BAr$^F{}_{24}$** are stable under vacuum toward NH_3 loss. Density Functional Theory (DFT) calculations[20] (see SI for details) predict the Ni–NH_3 binding energy of ΔG^o = −26.8 kcal mol^{-1} (Figure S31). Of particular importance, **2-PF$_6$** and **2-BAr$^F{}_{24}$** are stable in CD_2Cl_2 or fluorobenzene for days with no discernable changes to the ^{1}H NMR spectrum. However, **[2]$^+$** is surprisingly unstable in C_6D_6 and [D_8]THF.[21] Dissolving crystalline **2-PF$_6$** or **2-BAr$^F{}_{24}$** in these solvents leads to disproportionation of the hydrazine moiety with formation of **1-BAr$^F{}_{24}$** and gaseous products NH_3, N_2, and trace amounts of H_2 (*vide infra*).[22] **2-PF$_6$** exhibits similar characteristics but is insoluble in benzene.

Given the noted instability of **2-BAr$^F{}_{24}$**, we probed Ni-mediated hydrazine disproportionation in independent reactions by treating a solution of **1-BAr$^F{}_{24}$** with 30 equiv of anhydrous N_2H_4. These experiments showed that disproportionation occurs to form NH_3 and N_2 as the primary products, H_2 was generated in lesser amounts (see SI).

We assessed the competency of **1-PF$_6$** and **1-BAr$^F{}_{24}$** to catalyze the chemical oxidation of NH_3 to N_2 under ambient conditions and a reaction time of 24 h. We noted that the counter anion identity of **[1]$^+$** has a significant impact on catalytic performance (see SI for tabulated catalytic results). Using 3.1 μmol **1-PF$_6$**, 800 equiv ^{t}Bu$_3$ArO$^\bullet$ and 200 equiv NH_3 in dimethoxyethane (DME), ~11 equiv N_2 per Ni and a trace amount of H_2 were formed. Catalytic performance improved in reactions using 1.5 μmol **1-PF$_6$**, 1600 equiv ^{t}Bu$_3$ArO$^\bullet$ and 400 equiv of NH_3 in DME, affording ~28 equiv N_2 / Ni. By employing **1-BAr$^F{}_{24}$** as the precatalyst, up to 56 equiv N_2 / Ni in DME, and ~46 equiv N_2 / Ni in acetonitrile were produced. The dramatic counterion effect on catalytic activity in polar solvents is correlated with the decreased stability of **2-BAr$^F{}_{24}$**. Moreover, the reduced solubility of postulated dicationic intermediates formed in the catalytic cycle upon homodimerization (*vide infra*) may also impact catalysis. Although **1-BAr$^F{}_{24}$** is soluble in benzene, catalytic trials produced ~12 equiv

N_2 per Ni center. Headspace analysis by GC-MS of reactions performed in a Teflon valved NMR tube using $^{15}NH_3$ confirmed the formation of $^{15}N_2$ (*m/z* = 30) indicating the $^{15}N_2$ formed is derived from $^{15}NH_3$ (See SI).

Next, we examined the first N–H bond cleavage step and the N–N bond forming step en route to N_2 formation starting with **1^{15N}-BAr$^{F}_{24}$**. Scheme 2 describes the individual steps of a postulated catalytic cycle. Our mechanistic hypothesis asserted that H atom abstraction from **1^{15N}-BAr$^{F}_{24}$** (Scheme 2, panel A, step **A**) would generate a putative intermediate that could be described by the resonance structures [CpNi^{III}(IMes)($^{15}NH_2$)]$^+$ (**[Ni^{III}-^{15}NH$_2$]$^+$**) or [CpNi^{II}(IMes)($^{15}NH_2^{\bullet}$)]$^+$ (**[Ni^{II}-^{15}NH$_2^{\bullet}$]$^+$**). Subsequent bimolecular homocoupling would then form {[CpNi^{II}(IMes)]$_2$(η^1:η^1-$^{15}N_2H_4$)}$^{2+}$ (**3^{15N}-BAr$^{F}_{24}$**) (Scheme 2 panel A, step **B**).

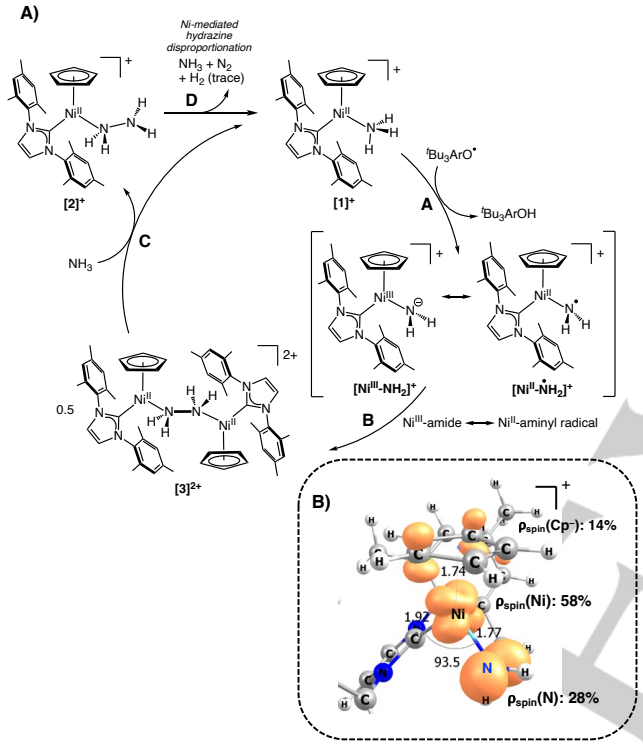

Scheme 2. A) Proposed catalytic cycle for NH_3 oxidation to N_2 using **[1]$^+$**. **B)** Spin density contour (at 0.005 $(e^-)^2$ Å^{-3}) and atomic distribution (ρ_{spin}) of a single unpaired electron in **[Ni^{III}-NH$_2$]$^+$** are from Hirshfeld analysis.[23] Calculated bond lengths [Å] and angle [°] shown for Ni–L (L = NH_2, C_{IMes}, ring centroid of Cp^-) and C_{IMes}–Ni–NH_2.

Addition of 2 equiv of the dark blue ^{t}Bu$_3$ArO$^{\bullet}$ to **1^{15N}-BAr$^{F}_{24}$** in CD_2Cl_2 generated a golden yellow solution and the formation of ^{t}Bu$_3$ArOH by ^{1}H NMR spectroscopy. The primary products observed in the $^{15}N\{^1H\}$ NMR spectrum showed **1^{15N}-BAr$^{F}_{24}$** and a new singlet resonance at δ -411 ppm assigned as **3^{15N}-BAr$^{F}_{24}$**. This resonance appears as a 1:2:1 triplet ($J_{1H\text{-}15N}$ = 70 Hz) in the ^{1}H coupled ^{15}N NMR spectrum as expected for the bridging ^{15}N-hydrazine ligand. The proton resonance (correlated by ^{1}H-^{15}N HSQC) of the bridging ^{15}N hydrazine moiety appear as a doublet centered at δ 1.82 ppm ($J_{1H\text{-}15N}$ = 70 Hz) in the ^{1}H NMR spectrum.[24],[25] Addition of excess $^{15}NH_3$ to the sample containing **3^{15N}-BAr$^{F}_{24}$** afforded free $^{15}N_2H_4$. The liberated $^{15}N_2H_4$ exhibits a cross peak in the ^{1}H-^{15}N HSQC spectrum at δ -341 ppm, corresponding to a ^{1}H resonance at δ 1.28 ppm.

The rapid consumption of ^{t}Bu$_3$ArO$^{\bullet}$ indicates homolytic cleavage of the first N–H bond is thermodynamically favorable. From the $BDFE_{O\text{-}H}$ values in Figure 1, we estimate the first $BDFE_{N\text{-}H}$ of **[1]$^+$** to be less than 76 kcal mol^{-1}. Thus, NH_3 N–H bond weakening[26] of ~28 kcal mol^{-1} occurs upon coordination to [CpNi(IMes)]$^+$ (free NH_3 $BDFE_{N\text{-}H}$ = 103.3 kcal mol^{-1} in gas phase; calculated to be 100.7 kcal mol^{-1} in Figure S32).[15b] Because the addition of a large excess H atom acceptors has been shown to overcome thermodynamically unfavorable reactions of ~7-12 kcal mol^{-1},[13] we examined the weaker H atom acceptor, TEMPO$^{\bullet}$, for NH_3 oxidation. In a reaction using 1.5 μmol **1-BAr$^{F}_{24}$**, 1600 equiv TEMPO$^{\bullet}$ ($BDFE_{OH}$ of TEMPO-H = 65.2 kcal mol^{-1} in benzene)[11] and 400 equiv of NH_3 in DME, ~15 equiv N_2 was formed per Ni center in 24 h.[27] While GC-MS analysis showed the formation of $^{15}N_2$ (*m/z* = 30) using **1^{15N}-BAr$^{F}_{24}$**, excess TEMPO$^{\bullet}$, and $^{15}NH_3$, the presence of $^{14}N^{15}N$ (*m/z* = 29) and O_2 (in GC traces of large scale runs) suggest TEMPO$^{\bullet}$ degradation may be occuring in Ni-catalyzed formation of N_2 from NH_3 (See SI).

DFT calculations probing the electronic structure of the product generated from abstraction of the first H atom from **[1]$^+$** in implicit polarizable solvent continuum[28] indicate this product is best described as a covalently coordinated amide ligand to a formally Ni^{3+} (3d^7) center (Scheme 2B, **[Ni^{III}-NH$_2$]$^+$**). Upon HAA, the electron hole created by the H atom abstraction relaxes into the metal d-manifold that creates a paramagnetic Ni center. The spin density contour plot in Scheme 2B, indicates three main localized contributions to the frontier orbital involved in HAT (see details in Table S6): (1) on two C atoms of the Cp^- ring (14% *via* σ interaction), (2) at the Ni center (58%, off-axis 3d-orbital), (3) on the N atom of the amide ligand (28% *via* π-interaction). In this frontier orbital description, the IMes ligand does not exhibit a localized contribution of spin density. Furthermore, the computed ionic and covalent Ni^{III}–$(NH_2)^-$ bond (1.77 Å) for **[Ni^{III}-NH$_2$]$^+$** was significantly shorter than the covalent bonding of Ni^{II}–NH_3 in **1-BAr$^{F}_{24}$** and Ni^{II}–N_2H_4 in **2-PF$_6$** (exp./calc.: 1.951/1.973 Å and 1.937/1.958 Å; respectively; Figure S34). The computed ~1/3 of an electron spin-density on the N atom of the amide ligand of **[Ni^{III}–NH$_2$]$^+$** indicates the presence of sufficient aminyl radical character to form the N–N bond *via* bimolecular homocoupling. The calculated free energy of 1 kcal mol^{-1} ($\Delta G^{o,dim}$ in Figure S33) to form **[3]$^{2+}$** suggests a spontaneous process for dimerization under catalytic conditions.

The presence of exogenous NH_3 facilitates the dissociation of **3-BAr$^{F}_{24}$** into the precatalyst **1-BAr$^{F}_{24}$** and end-on bound hydrazine complex **2-BAr$^{F}_{24}$** (Scheme 2, panel A, step **C**). DFT calculations predict the dissociation step is highly spontaneous ($\Delta G^{o,dis}$ = ~-28 kcal mol^{-1}; Figure S33).

In the final step of the catalytic cycle, the intrinsic instability of **2-BAr$^{F}_{24}$** towards hydrazine disproportionation is postulated to play a critical role in N_2 formation. **2-BAr$^{F}_{24}$** is unstable in most solvents other than CH_2Cl_2, and disproportionation generates **1-BAr$^{F}_{24}$** with the liberation of gaseous products N_2, NH_3, and H_2 (Scheme 2 panel A, step **D**). However, under catalytic conditions (with excess NH_3 and ^{t}Bu$_3$ArO$^{\bullet}$ present), alternative reaction pathways were considered: (1) **3-BAr$^{F}_{24}$** could react with excess ^{t}Bu$_3$ArO$^{\bullet}$ to generate a nickel diazene (Ni–N_2H_2) product. Free diazene or a metal-bound diazene species can undergo disproportionation forming ½ N_2 and ½ N_2H_4 as Peters and coworkers recently described for another Ni complex (Figure 1b).[17] In the present case, *in situ* diazene formation and disproportionation cannot be ruled out based on the quantified gaseous products formed in catalysis; (2) as noted above, treatment of **3^{15N}-BAr$^{F}_{24}$** with excess NH_3, liberated free hydrazine presumably by ligand exchange with **2-BAr$^{F}_{24}$** generating **1-**

BAr$^{F}_{24}$. Free hydrazine could undergo disproportionation in solution with excess $^{t}Bu_3ArO^{\bullet}$ present under catalytic conditions. However, independent experiments showed the addition of $^{t}Bu_3ArO^{\bullet}$ to a THF solution of hydrazine led to the discrete formation of N_2 and H_2 (See SI). Since H_2 formation is very low in catalytic trials, the disproportionation of free hydrazine may be only be a nominal reaction; (3) an intramolecular N–N bond coupling mechanism (Figure S32) involving a high-spin paramagnetic, formally 20e- complex $[CpNi(IMes)(NH_3)_2]^+$ is energetically not competitive with the homodimerization step based on DFT calculations (Figure S33). The speciation of the Ni complex following catalysis has not been determined. Catalytic reactions performed for 48 h did not result in an increase of N_2 formation suggesting degradation of the Ni catalyst may be occurring.

In summary, we described catalytic NH_3 oxidation to N_2 by HAA mediated by Ni complexes that takes advantage of unstable hydrazine and/or diazene intermediates to generate N_2. The Ni-NH_3 N-H bond in **[1]$^{+}$**, is estimated to have a $BDFE_{N\text{-}H}$ of less than 76 kcal mol^{-1} permitting the use of $^{t}Bu_3ArO^{\bullet}$ or TEMPO$^{\bullet}$ radicals in catalytic NH_3 oxidation. Importantly, the balance of N-H bond weakening in the Ni-NH_3 complex and the partial aminyl radical character of the Ni-NH_2 product are critical features for catalysis in this Ni system. Using $^{t}Bu_3ArO^{\bullet}$, bimolecular homocoupling of two Ni-NH_2 species generates a $Ni^{II}_2(N_2H_4)$ complex denoting the N-N bond forming step in the proposed catalytic cycle. Future efforts will focus on modifications of the ancillary ligands to improve catalyst stability and will explore this Ni system for electrocatalytic NH_3 oxidation to N_2.

Acknowledgements

The authors thank Dr. Brian Tripet for assistance with NMR experiments, and Dr. Donald Smith for assistance with GC-MS analysis. This material is based upon work supported by the National Science Foundation under Grant No. 1956161 and, in-part, start-up funding from Montana State University. Support for MSU's NMR Center and the 400 MHz NMR spectrometer used in this research has been provided by the National Science Foundation (Grant No. NSF-MRI: CHE-2018388) and MSU's office of the Vice President for Research and Economic Development. Funding for MSU Proteomics, Metabolomics and Mass Spectrometry Facility was made possible in part by the MJ Murdock Charitable Trust and the National Institute of General Medical Sciences of the National Institutes of Health under Award Number P20GM103474. The authors gratefully acknowledge financial support for the X-ray diffractometer from the NSF (CHE 0619920) and the Institutional Development Award (IDeA) from the National Institute of General Medical Sciences of the National Institutes of Health (Grant # 2P20GM103432). Computational resources were provided by the Extreme Science and Engineering Discovery Environment (XSEDE, supported by National Science Foundation, Grant No. CHE210021). This research was also supported in part through computational resources and services provide by Advanced Research Computing at the University of British Columbia.

Keywords: nickel • ammonia oxidation • molecular catalyst • dinitrogen • hydrogen atom abstraction

References

[1] (a) N. Salmon, R. Bañares-Alcántara, *Sustainable Energy Fuels* **2021**, *5*, 2814-2839; (b) R. H. Dolan, J. E. Anderson, T. J. Wallington, *Sustainable Energy Fuels* **2021**, *5*, 4830-4841; (c) S. Giddey, S. P. S. Badwal, C. Munnings, M. Dolan, *ACS Sustainable Chem. Eng.* **2017**, *5*, 10231-10239; (d) Y. Zhao, B. P. Setzler, J. Wang, J. Nash, T. Wang, B. Xu, Y. Yan, *Joule* **2019**, *3*, 2472-2484; (e) A. Valera-Medina, H. Xiao, M. Owen-Jones, W. I. F. David, P. J. Bowen, *Prog. Energy and Combust. Sci.* **2018**, *69*, 63-102.

[2] (a) J. W. Erisman, M. A. Sutton, J. Galloway, Z. Klimont, W. Winiwarter, *Nat. Geosci.* **2008**, *1*, 636-639; (b) C. Smith, A. K. Hill, L. Torrente-Murciano, *Energy Environ. Sci.* **2020**, *13*, 331-344.

[3] H. L. Du, M. Chatti, R. Y. Hodgetts, P. V. Cherepanov, C. K. Nguyen, K. Matuszek, D. R. MacFarlane, A. N. Simonov, *Nature* **2022**, *609*, 722-727.

[4] (a) C. H. Christensen, T. Johannessen, R. Z. Sørensen, J. K. Nørskov, *Catal. Today* **2006**, *111*, 140-144; (b) J. G. Chen, R. M. Crooks, L. C. Seefeldt, K. L. Bren, R. M. Bullock, M. Y. Darensbourg, P. L. Holland, B. Hoffman, M. J. Janik, A. K. Jones, M. G. Kanatzidis, P. King, K. M. Lancaster, S. V. Lymar, P. Pfromm, W. F. Schneider, R. R. Schrock, *Science* **2018**, *360*, No. eaar6611.

[5] (a) K. E. Lamb, M. D. Dolan, D. F. Kennedy, *Int. J. Hydrogen Energy* **2019**, *44*, 3580-3593; (b) O. Elishav, B. Mosevitzky Lis, E. M. Miller, D. J. Arent, A. Valera-Medina, A. Grinberg Dana, G. E. Shter, G. S. Grader, *Chem. Rev.* **2020**, *120*, 5352-5436.

[6] P. L. Dunn, B. J. Cook, S. I. Johnson, A. M. Appel, R. M. Bullock, *J. Am. Chem. Soc.* **2020**, *142*, 17845-17858.

[7] F. Habibzadeh, S. L. Miller, T. W. Hamann, M. R. Smith III, *Proc. Natl. Acad. Sci. U. S. A.* **2019**, *116*, 2849-2853.

[8] (a) M. J. Trenerry, C. M. Wallen, T. R. Brown, S. V. Park, J. F. Berry, *Nat. Chem.* **2021**, *13*, 1221-1227; (b) J. Holub, N. Vereshchuk, F.-J. Sánchez-Baygual, M. Gil-Sepulcre, J. Benet-Buchholz, A. Llobet, *Inorg. Chem.* **2021**, *60*, 13929-13940; (c) K. Nakajima, H. Toda, K. Sakata, Y. Nishibayashi, *Nat. Chem.* **2019**, *11*, 702-709.

[9] (a) M. D. Zott, P. Garrido-Barros, J. C. Peters, *ACS Catal.* **2019**, *9*, 10101-10108; (b) M. D. Zott, J. C. Peters, *J. Am. Chem. Soc.* **2021**, *143*, 7612-7616; (c) Y. Li, J. Y. Chen, Q. Miao, X. Yu, L. Feng, R. Z. Liao, S. Ye, C. H. Tung, W. Wang, *J. Am. Chem. Soc.* **2022**, *144*, 4365-4375.

[10] H. Toda, K. Kuroki, R. Kanega, S. Kuriyama, K. Nakajima, Y. Himeda, K. Sakata, Y. Nishibayashi, *ChemPlusChem* **2021**, *86*, 1511-1516.

[11] J. J. Warren, T. A. Tronic, J. M. Mayer, *Chem. Rev.* **2010**, *110*, 6961-7001.

[12] (a) P. Bhattacharya, Z. M. Heiden, E. S. Wiedner, S. Raugei, N. A. Piro, W. S. Kassel, R. M. Bullock, M. T. Mock, *J. Am. Chem. Soc.* **2017**, *139*, 2916-2919; (b) B. J. Cook, S. I. Johnson, G. M. Chambers, W. Kaminsky, R. M. Bullock, *Chem. Commun.* **2019**, *55*, 14058-14061; (c) B. J. Cook, M. Barona, S. I. Johnson, S. Raugei, R. M. Bullock, *Inorg. Chem.* **2022**, *61*, 11165-11172; (d) Z. Wang, S. I. Johnson, G. Wu, G. Menard, *Inorg. Chem.* **2021**, *60*, 8242-8251.

[13] P. Bhattacharya, Z. M. Heiden, G. M. Chambers, S. I. Johnson, R. M. Bullock, M. T. Mock, *Angew. Chem. Int. Ed.* **2019**, *58*, 11618-11624.

[14] P. L. Dunn, S. I. Johnson, W. Kaminsky, R. M. Bullock, *J. Am. Chem. Soc.* **2020**, *142*, 3361-3365.

[15] (a) J. E. Nutting, M. Rafiee, S. S. Stahl, *Chem. Rev.* **2018**, *118*, 4834-4885; (b) R. G. Agarwal, S. C. Coste, B. D. Groff, A. M. Heuer, H. Noh, G. A. Parada, C. F. Wise, E. M. Nichols, J. J. Warren, J. M. Mayer, *Chem. Rev.* **2022**, *122*, 1-49.

[16] H. Y. Liu, H. M. C. Lant, J. L. Troiano, G. Hu, B. Q. Mercado, R. H. Crabtree, G. W. Brudvig, *J. Am. Chem. Soc.* **2022**, *144*, 8449-8453.

[17] N. Gu, P. Oyala, J. Peters, *Angew. Chem. Int. Ed.* **2021**, *60*, 4009-4013.

[18] C. D. Abernethy, A. H. Cowley, R. A. Jones, *J. Organomet. Chem.* **2000**, *596*, 3-5.

[19] Deposition numbers 2206175 (for **1-PF$_6$**), 2206176 (for **1-BAr$^{F}_{24}$**), and 2206177 (for **2-PF$_6$**) contain the supplementary crystallographic data for this paper. These data are provided free of charge by the joint Cambridge Crystallographic Data Centre and Fachinformationszentrum Karlsruhe Access Structures service.

[20] J.-D. Chai, M. Head-Gordon, *Phys. Chem. Chem. Phys.* **2008**, *10*, 6615-6620.
[21] We rationalize that the instability of $\mathbf{2}^{+}$ toward the reductively promoted disproportionation of hydrazine may be attributed to a difference in the oxidation potential of $\mathbf{2}^{+}$ in various solvents as electron transfer is likely required to initiate the N−N bond cleavage of hydrazine.
[22] C. Köthe, B. Braun, C. Herwig, C. Limberg, *Eur. J. Inorg. Chem.* **2014**, 5296-5303.
[23] F. L. Hirshfeld, *Theor. Chim. Acta* **1977**, *44*, 129-138.
[24] Formation of a Ni-NH_2 (amido) product has been ruled out based on ^{1}H and ^{15}N spectroscopic data. See reference 25 for reported Ni-NH_2 complexes.
[25] (a) J. Cámpora, P. Palma, D. del Río, M. M. Conejo, E. Alvarez, *Organometallics* **2004**, *23*, 5653-5655; (b) D. Adhikari, S. Mossin, F. Basuli, B. R. Dible, M. Chipara, H. Fan, J. C. Huffman, K. Meyer, D. J. Mindiola, *Inorg. Chem.* **2008**, *47*, 10479-10490; (c) T. J. Schmeier, A. Nova, N. Hazari, F. Maseras, *Chem. Eur. J.* **2012**, *18*, 6915-6927; (d) D. V. Gutsulyak, W. E. Piers, J. Borau-Garcia, M. Parvez, *J. Am. Chem. Soc.* **2013**, *135*, 11776-11779; (e) R. M. Brown, J. Borau Garcia, J. Valjus, C. J. Roberts, H. M. Tuononen, M. Parvez, R. Roesler, *Angew. Chem. Int. Ed.* **2015**, *54*, 6274-6277; (f) A. H. Mousa, J. Bendix, O. F. Wendt, *Organometallics* **2018**, *37*, 2581-2593.
[26] (a) N. G. Boekell, R. A. Flowers II, *Chem. Rev.* **2022**, *122*, 13447-13477; (b) A. Wong, A. Chakraborty, D. Bawari, G. Wu, R. Dobrovetsky, G. Menard, *Chem. Commun.* **2021**, *57*, 6903-6906.
[27] O_2 was consistently observed during quantification of headspeace gases in catalytic trials using TEMPO. While we believe TEMPO to be the source of the O_2, this has not been experimentally verified by isotope labeling. Therefore, the O_2 was treated as contamination from air, and N_2 was subtracted accordingly to obtain the reported catalytic results.
[28] (a) M. Mammen, E. I. Shakhnovich, J. M. Deutch, G. M. Whitesides, *J. Org. Chem.* **1998**, *63*, 3821-3830; (b) A. V. Marenich, C. J. Cramer, D. G. Truhlar, *J. Phys. Chem. B* **2009**, *113*, 6378-6396.

Entry for the Table of Contents

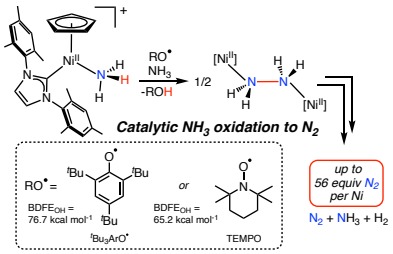

A nickel complex for catalytic oxidation of NH_3 to N_2 is demonstrated using the radicals 2,4,6-tri-*tert*-butylphenoxyl ($^tBu_3ArO^•$) or 2,2,6,6-(tetramethylpiperidine-1-yl)oxyl (TEMPO) as the H-atom acceptor to cleave the N-H bond of a NH_3 ligand. Two Ni-NH_2 fragments form an N–N bond in a bridging Ni-hydrazine product. Ni-mediated hydrazine disproportionation affords N_2 and NH_3 in the proposed catalytic cycle. (BDFE = Bond Dissociation Free Energy)